Redox Biology 17 (2018) 246–258

Contents lists available at ScienceDirect

Redox Biology

journal homepage: www.elsevier.com/locate/redox

Research Paper

High CD44 expression mediates p62-associated NFE2L2/NRF2 activation in breast cancer stem cell-like cells: Implications for cancer stem cell resistance

In-geun Ryoo[a], Bo-hyun Choi[b], Sae-Kwang Ku[c], Mi-Kyoung Kwak[a,b,d,*]

[a] Integrated Research Institue for Pharmaceutical Sciences, The Catholic University of Korea, 43 Jibong-ro, Bucheon, Gyeonggi-do 14662, Republic of Korea
[b] Department of Pharmacy and BK21 PLUS Team for Creative Leader Program for Pharmacomics-based Future Pharmacy, Graduate School of The Catholic University of Korea, Republic of Korea
[c] College of Korean Medicine, Daegu Haany University, Gyeongsan, Gyeonsangbuk-do 712-715, Republic of Korea
[d] College of Pharmacy, The Catholic University of Korea, Republic of Korea

ARTICLE INFO

Keywords:
CD44
Cancer stem cell (CSC)
NFE2L2/NRF2
Reactive oxygen species (ROS)
Stress resistance
p62

ABSTRACT

Cluster of differentiation 44 (CD44) is the most common cancer stem cell (CSC) marker and high CD44 expression has been associated with anticancer drug resistance, tumor recurrence, and metastasis. In this study, we aimed to investigate the molecular mechanism by which CD44 and nuclear factor erythroid 2-like 2 (NFE2L2; NRF2), a key regulator of antioxidant genes, are linked to CSC resistance using $CD44^{high}$ breast CSC-like cells. NRF2 expression was higher in $CD44^{high}$ cell populations isolated from doxorubicin-resistant MCF7 (ADR), as well as MCF7, MDA-MB231, and A549 cells, than in corresponding $CD44^{low}$ cells. High NRF2 expression in the $CD44^{high}CD24^{low}$ CSC population (ADR44P) established from ADR cells depended on standard isoform of CD44. Silencing of *CD44* or overexpression of CD44 resulted in the reduction or elevation of NRF2, respectively, and treatment with hyaluronic acid, a CD44 ligand, augmented NRF2 activation. As functional implications, *NRF2* silencing rendered ADR44P cells to retain higher levels of reactive oxygen species and to be sensitive to anticancer drug toxicity. Moreover, *NRF2*-silenced ADR44P cells displayed tumor growth retardation and reduced colony/sphere formation and invasion capacity. In line with these, CD44 significantly colocalized with NRF2 in breast tumor clinical samples. The molecular mechanism of CD44-mediated NRF2 activation was found to involve high p62 expression. CD44 elevation led to an increase in p62, and inhibition of p62 resulted in NRF2 suppression in ADR44P. Collectively, our results showed that high CD44 led to p62-associated NRF2 activation in $CD44^{high}$ breast CSC-like cells. NRF2 activation contributed to the aggressive phenotype, tumor growth, and anticancer drug resistance of $CD44^{high}$ CSCs. Therefore, the CD44-NRF2 axis might be a promising therapeutic target for the control of stress resistance and survival of $CD44^{high}$ CSC population within breast tumors.

1. Introduction

Cancer stem cells (CSCs), a small population of cancer cells, possess self-renewal and differentiation capacity similar to normal stem cells. In 1997, Bonnet and Dick observed that only the $CD34^{+}/CD38^{-}$ cells from acute myeloid leukemia (AML) patients were capable of tumor initiation in immune-deficient mice [1]. Since this discovery, CSCs have been identified in other types of cancer, including breast, brain, and lung cancer, and they are believed to be responsible for tumor relapse after therapy [2–4]. One common property between adult stem cells and CSCs is a low level of reactive oxygen species (ROS). Hematopoietic stem cells retain a lower level of ROS than their mature lineage, and this low ROS level is associated with stem-cell resistance to an oxidative environment [5,6]. Like hematopoietic stem cells, CSC subpopulations from several human as well as murine breast tumors contained lower ROS levels than corresponding non-tumor cells [7]. Because of the low ROS level, CSCs were relatively more resistant to radiation-induced DNA damage and cell death than non-tumor cells. Diehn *et al.* [7] also found that breast CSCs express high levels of antioxidant proteins, such as glutathione peroxidase-1 (GPX1), catalase, and superoxide dismutase-2 (SOD2) when compared to non-tumor cells, indicating a differential expression of ROS-scavenging genes in CSCs. In addition,

Abbreviations: AKR, aldo-keto reductase; ARE, antioxidant response element; CD44, cluster of differentiation 44; CSC, cancer stem cell; GCLC, glutamate-cysteine ligase catalytic subunit; GPX, glutathione peroxidase; GSH, glutathione; HO-1, heme oxygenase-1; HA, hyaluronic acid; KEAP1, Kelch-like ECH-associated protein 1; MAPK, mitogen-activated protein kinase; MDR1, multidrug resistance protein 1; NFE2L2/NRF2, nuclear factor erythroid 2-like 2; NQO-1, NAD(P)H quinone oxidoreductase-1; OCT4, octamer-binding transcription factor 4; PI3K, phosphoinositide 3-kinase; ROS, reactive oxygen species; SOD, superoxide dismutase; SOX2, sex determining region Y-box 2

* Correspondence to: College of Pharmacy, The Catholic University of Korea, 43 Jibong-ro, Wonmi-gu, Bucheon, Gyeonggi-do 14662, Republic of Korea.
E-mail address: mkwak@catholic.ac.kr (M.-K. Kwak).

https://doi.org/10.1016/j.redox.2018.04.015
Received 21 February 2018; Received in revised form 6 April 2018; Accepted 13 April 2018
Available online 26 April 2018

enhanced expression of genes encoding ROS metabolism and drug efflux transporters elicited CSC resistance against anticancer treatment [8–10].

The multifunctional glycoprotein cluster of differentiation 44 (CD44) is a receptor for extracellular matrix (ECM) components, primarily hyaluronic acid (HA), and is the most common CSC marker in multiple types of cancers. This cell-surface glycoprotein, encoded by a single and highly conserved gene, exists in a variety of isoforms resulting from alternative splicing and post-translational modification [11,12]. Among these, the standard isoform (CD44s), which is the smallest CD44 isoform, is encoded exclusively by the constant exons. Inclusion of the variant exons that are located between the constant exons produces CD44 variant isoforms (CD44v). CD44s is widely expressed in most animal cells, whereas CD44v is present only on some epithelial cells, including malignant epithelial cells [11,12]. Although CD44 is involved in normal physiological events, such as cell-cell interaction and cell-matrix interaction, its high expression has been associated with tumor initiation and progression. Through the binding to cytoskeletal proteins, CD44 induces actin-cytoskeletal remodeling, which is involved in cancer cell motility, migration, and invasion [13]. Particularly, lines of evidence indicate that high CD44 expression is related to the CSC phenotype in many types of tumors. As few as 100 $CD44^+$ cells from breast tumors were found to be capable of initiating a heterogeneous tumor in vivo, and a single $CD44^+$ cell isolated from xenograft tumors demonstrated self-renewal properties when transplanted into mice [14,15]. $CD44^{high}$ prostate cancer cells showed increased mRNA levels of the stemness marker octamer-binding protein 3/4 (OCT3/4) and β-catenin, and had stronger proliferative, tumorigenic, and metastatic capacity than the corresponding $CD44^{low}$cells [16]. $CD44^{high}$ gastric cancer cells were reported to be resistant to cisplatin and 5-fluorouracil chemotherapy and to upregulate hedgehog signaling, which promotes the CSC phenotype [17]. As mentioned earlier, numerous studies have shown that CD44 is the most reliable CSC marker in multiple types of tumors; however, the molecular function of CD44 for the CSC phenotype is not fully understood.

Nuclear factor erythroid 2-like 2 (NFE2L2/NRF2) protects cells against oxidative damage by upregulating the expression of various genes encoding multiple antioxidant proteins (e.g., glutathione [GSH] synthesis and regeneration enzymes), phase 2 detoxifying enzymes (e.g., aldo-keto reductase [AKR]), and drug efflux transporters [18,19]. When cells are exposed to oxidative stress, NRF2 dissociates from its inhibitor Kelch-like ECH-associated protein 1 (KEAP1), and this allows NRF2 to translocate into the nucleus where it binds to the antioxidant-response elements (AREs) in its target genes [20,21]. In addition to KEAP1-mediated regulation, p62 is involved in NRF2 activation as a non-canonical regulation pathway. Originally, p62 was identified as a linker protein that associates ubiquitinated proteins with the autophagy system, and is now getting attention for its role in ROS defense. Specifically, p62 protein has been found to bind to specific KEAP1 residues by competing with NRF2 and thereby, p62 elevation can result in NRF2 elevation [22,23]. Additionally, p62 has been shown to induce autophagic degradation of KEAP1 protein, which also leads to p62-mediated NRF2 activation [24].

Over the last few decades, numerous studies have focused on the protective effects of NRF2 in normal cells [25,26]. However, accumulating evidence suggests that NRF2 hyperactivation provides a favorable environment for cancer cells to facilitate tumor growth and survival. High NRF2 expression in cancer cells could result in growth enhancement and chemoresistance by upregulating its target genes, including GSH-generating enzymes and drug efflux transporters [27,28]. Our previous studies also showed that *NRF2* silencing in different types of cancer cells could decrease tumor growth and enhanced sensitivity to anticancer treatments [29–31]. In particular, considering the direct involvement of NRF2 in cellular ROS regulation and anticancer drug resistance, the possible contribution of NRF2 to CSC biology remains to be addressed. We previously showed that constitutive activation of NRF2 was closely correlated with anticancer drug resistance in CSC-enriched spheroid breast and colon cancer cells [32,33]. In this study, in an attempt to investigate the direct association of NRF2 with CSC phenotype, we established a $CD44^{high}$ breast CSC-like system, and investigated the role of NRF2 activation in CSC-like properties in breast CSCs.

2. Materials and methods

2.1. Reagents

Antibodies recognizing sex determining region Y-box 2 (SOX2), octamer-binding transcription factor 4 (OCT4), p62, microtubule-associated proteins 1A/1B light chain 3B (LC3B), multidrug resistance protein-1 (MDR1), glyceraldehyde 3-phosphate dehydrogenase (GAPDH), and CD44 were from Cell Signaling Technology (Danvers, MA, USA). NRF2, KEAP1, lamin B and β-tubulin antibodies were obtained from Santa Cruz Biotechnology (Santa Cruz, CA, USA). Fluorescein isothiocyanate (FITC)-conjugated CD44 and phycoerythrin (PE)-conjugated CD24 antibodies were from Biolegend (San Diego, CA, USA). The CD44s plasmid was obtained from Addgene (Cambridge, MA, USA). The lentiviral expression plasmids for human *NRF2* short hairpin RNA (shRNA), Mission™ Lentiviral Packaging Mix, hexadimethrine bromide, puromycin, doxorubicin, daunorubicin, hyaluronic acid, 4-methylumbelliferone and 3-(4,5-dimethylthiazol-2-yl)-2,5-diphenyltetrazolium bromide (MTT) were from Sigma-Aldrich (Saint Louis, MO, USA). Propidium iodide (PI) was purchased from Biolegend. 6-Carboxy-2',7'-dichlorodihydrofluorescein diacetate (carboxy-H_2DCFDA) were purchased from Life Technologies (Carlsbad, CA, USA). The SYBR premix ExTaq system was obtained from Takara (Otsu, Japan). Cyto-ID autophagy detection kit 2.0 was obtained from Enzo Life Science (Farmingdale, NY, USA).

2.2. Cell culture

The human breast carcinoma cell line MCF7 and MDA-MB231 were purchased from the American Type Culture Collection (Rockville, MD, USA). Doxorubicin-resistant cell line MCF7/ADR was gifted by Dr. Keon Wook Kang (Seoul National University, Republic of Korea). These cells were maintained in Dulbecco's modified Eagle's medium (DMEM) (HyClone, Logan, UT, USA) with 10% fetal bovine serum (FBS; HyClone) and penicillin/streptomycin (WelGene Inc., Daegu, Republic of Korea). The human lung carcinoma cell line A549 was obtained from ATCC. These cells were maintained in RPMI 1640 with 10% fatal bovine serum and penicillin/streptomycin. The cells were grown at 37 °C in a humidified 5% CO_2 atmosphere.

2.3. Sphere culture of cancer cells

Cells were plated at a density of 20,000 cells/mL in 100 mm ultralow attachment plates (Corning Costar Corp., Cambridge, MA, USA) and were grown in a serum-free DMEM and Nutrient Mixture F-12 medium supplemented with B27 (1:50, Life Technologies), 20 ng/mL epithelial growth factor (EGF), 20 ng/mL basic fibroblast growth factor (R&D System, Minneapolis, MN, USA), 5 μg/mL bovine insulin (Cell Application Inc., San Diego, CA, USA), 0.5 μg/mL hydrocortisone (Sigma-Aldrich), and penicillin/streptomycin (HyClone) as described previously [34]. Cells were grown for 3 days for sphere formation.

2.4. Production of shRNA lentiviral particles

Lentiviral particles were produced in HEK 293T cells following the transfection of the cells with the relevant shRNA expression plasmid and Mission™ Lentiviral Packaging Mix as described previously [35]. Briefly, HEK 293T cells in Opti-MEM (Life Technologies) were transfected with 1.5 μg pLKO.1-*NRF2* shRNA, (5′-CCGGGCTCCTACTGTGAT

GTGAAATCTCGAGATTTCACATCACAGTAGGA-3′) with packaging mix using Lipofectamine 2000 (Life Technologies). As a nonspecific RNA, the pLKO.1-scrambled (sc) RNA plasmid was transfected in the control group. The next day, the medium containing the transfection complex was removed and lentiviral particles were harvested after 4 days.

2.5. Establishment of NRF2 knockdown cells

Cells in 6-well plates were transduced with lentiviral particles containing the nonspecific pLKO.1-scRNA (sc) or pLKO.1-*NRF2* shRNA (shNRF2) in the presence of 8 μg/mL hexadimethrine bromide. Transduction was continued for 48 h and followed by a 24 h-recovery in complete medium as described previously [34]. For the selection of stable transgene-expressing cells, puromycin (2 μg/mL) incubation was continued for up to 4 weeks.

2.6. Total RNA extraction and reverse transcriptase (RT)-polymerase chain reaction (PCR) analysis

Total RNA was isolated from the cells using the TRIzol reagent (Life Technologies). For the synthesis of cDNA, RT reactions were performed by incubating 200 ng of total RNA with a reaction mixture containing 0.5 μg/μL oligo $dT_{12–18}$ and 200 U/μL moloney murine leukemia virus RT (Life Technologies). Real-time RT-PCR was carried out using a Roche Light Cycler (Mannheim, Germany) with the Takara SYBR Premix ExTaq System for relative quantification. Primers were synthesized by Bioneer (Daejeon, Republic of Korea) and primer sequences for the human genes are described in our previous studies [29,36] . For *CD44* isoforms amplification, PCR was carried out with a thermal cycler (Bio-Rad, Hercules, CA, USA) and PCR products were resolved on 3% agarose gels and the images were captured by using a Gel Doc EZ Imager (Bio-Rad). PCR primers for *CD44* isoforms are as follows: *CD44* 5′-CGGACACCATGGACAAGTTT-3′ and 5′- GAAAGCCTTGCAGAGGT CAG-3′; *CD44s* 5′-AGCAGCGGCTCCTCCAGTGA-3′ and 5′- CCCACTGG GGTGGAATGTGTCT-3′; CD44v3 5′-GCACTTCAGGAGGAGGTTAC ATC-3′ and 5′-CTGAGGTGTCTGTCTCTTTC-3′; CD44v8-10 5′-TCCCAG ACGAAGACAGTCCCTGGAT-3′ and 5′-CACTGGGGTGGAATGTGTCTTG GTC -3′.

2.7. MTT assay

Viable cell numbers were determined by MTT assay. MCF7 cells were seeded at a density of 5×10^3 cells/well in 96-well plates and incubated with the relevant compounds (doxorubicin, 5-FU or H2O2) for the indicated times. MTT solution (2 mg/mL) was added to the cells and further incubated for 4 h. The MTT solution was removed, 100 μL/well of DMSO was added, and the absorbance was measured at 540 nm using a SPECTRO $Star^{Nano}$ (BMG LABTECH GmbH, Allmendgruen, Ortenberg, Germany).

2.8. Immunoblot analysis

Cells were lysed with radioimmunoprecipitation assay (RIPA) lysis buffer (50 mM Tris [pH 7.4], 150 mM NaCl, 1 mM EDTA, and 1% NP40) containing a protease inhibitor cocktail (Sigma–Aldrich). Nuclear and cytoplasmic fractions were prepared using the NE-PER® Nuclear and Cytoplasmic Extraction reagents according to the manufacturer's instructions. The protein concentration was determined using a bicinchoninic acid assay (BCA) kit (Thermo Scientific, Middletown, VA, USA). The protein samples were separated by electrophoresis on 6–12% SDS-polyacrylamide gels and transferred to nitrocellulose membranes (Whatman GmbH, Dassel, Germany) using a Trans-Blot Semi-Dry Cell (Bio-Rad). The membrane was blocked with 3% BSA for 1 h, and then incubated with the antibodies. Following the addition of the enhanced chemiluminescence reagent (Thermo Scientific), images were detected using a GE Healthcare LAS-4000 mini imager (GE Healthcare Life Sciences, Piscataway, NJ, USA).

2.9. Immunocytochemical Analysis

Cells were plated at a density of 5×10^3 cells/well on cover glass slides. The cells were washed with cold PBS three times and were fixed in cold methanol for 10 min. Then, anti-CD44 antibody (1:200) was incubated in fixed cells at 4 °C overnight. The next day, the cells were washed with PBS and the Alexa Fluor 488 goat anti- rabbit antibody (1:500) incubation was performed at room temperature for 1 h. For nuclear staining, Hoechst 33342 incubation was executed for 10 min. Fluorescent images were obtained using the LSM 710 confocal microscopy (Carl Zeiss, Jena, Germany).

2.10. Cyto-ID autophagy detection

Cyto-ID autophagy detection kit was used to detect autophagy vacuoles and monitor autophagic flux in live cells. Cells were plated at a density of 1×10^5 cells/plate in 60 mm plates and treated with rapamycin (500 nM, positive control) for 24 h. Next, cells were washed with PBS and harvested with trypsin. For autophagic vacuole detection, cells were stained with Cyto-ID dye according to the manufacturer's instructions. Autophagic vacuoles were measured using a 488 nm laser source in a Becton-Dickinson FACSCanto and data were analyzed with FACSDiva software (Becton-Dickinson, SanJose, CA, USA)

2.11. Measurement of ROS

Cellular ROS levels were determined using the fluorescent carboxy-H_2DCFDA as described previously [37]. Briefly, cells were incubated with 30 μM carboxy-H_2DCFDA for 30 min and fluorescence was measured using a 488 nm laser source in a Becton-Dickinson FACSCanto. Data were analyzed with FACSDiva software.

2.12. siRNA Transfection

Predesigned siRNA for *NRF2*, *p62*, and *CD44*, and a scrambled control siRNA were obtained from Bioneer. The cells were seeded in 60 mm plates at a density of 3–5 x 10^4 cells and grown overnight. The next day, cells were transfected with siRNA using a Lipofectamine 2000 reagent (Life Technologies).

2.13. CD44s overexpression

Retroviral particles were produced in HEK 293T cells following the transfection of the cells with the CD44s retroviral expression plasmid (pBabe-CD44s, Addgene) or the empty vector (pBabe) and Retrovirus Packaging Kit Ampho (Takara) as described by the manufacturer. MCF7 cells in 6-well plates were transduced with retroviral particles containing the blank pBabe or pBabe-CD44s plasmid in the presence of 8 μg/mL hexadimethrine bromide. Transduction was continued for 48 h and followed by a 24 h-recovery in complete medium. For the selection of stable transgene-expressing cells, puromycin (2 μg/mL) incubation was continued for up to 4 weeks.

2.14. Flow cytometry and cell sorting

Cells were dissociated using 0.05% trypsin-ethylenediaminetetraacetic acid (EDTA) solution and resuspended in PBS containing 2% FBS. Cells were washed with cold-PBS and stained with FITC-conjugated CD44 or PE-conjuated CD24 antibody for 30 min. Cells were washed and analyzed using a Becton-Dickinson FACSCanto for the determination of cell population distribution. $CD44^{high}$ and $CD44^{low}$ populations from MCF7, MCF7/ADR, MDAMB-231, and A549 cells were sorted using a BD FACS Aria III (Becton-Dickinson).

2.15. Soft agar colony formation assay

To evaluate the anchorage-independent growth ability of cancer cells, soft agar colony formation assay was performed. 3 x 10^3 cells were suspended in top soft agar layer (0.35% soft agar) and seeded into 6 well plates precoated with 0.5% base agar. Colonies were allowed to grow at 37 °C in a 5% CO_2 incubator for 2–3 weeks, and colony number was counted using an ECLIPSE Ti inverted microscope and the NIS-Elements AR (V. 4.0) computer software program (NIKON Instruments Korea, Seoul, Republic of Korea) [38].

2.16. Cell invasion assay

The transwell cell migration and invasion were assayed using the BioCoat Matrigel invasion chambers with 8.0 μm polyethylene terephthalate (PET) membrane in 24-well plate format (Corning). Warm culture medium was added to the inserts and well plates for rehydration for 2 h at 37 °C. For the invasion assay, 5000 cells were seeded on the insert and the well plate was filled with 750 μL of medium supplemented with 10% FBS. After 24 h incubation, the cells on the lower surface of the insert were fixed by adding 4% paraformaldehyde for 10 min and stained with 0.5% crystal violet for 15 min. After removal of crystal violet stain, invasive cells were counted using the light microscopy [39].

2.17. Tumor xenograft assay

MCF7 and ADR44P cells were grown overnight and harvested, washed with PBS. The suspension of 2.5 × 10^6 cells in 0.2 mL serum-free medium was injected subcutaneously into the flank of 6-weeks-old BALBc (*nu/nu*) mice (Orient Bio. Inc., Gyeonggi-do, Republic of Korea), which were maintained in pathogen-free environment. The tumor growth was measured from 7 to 14 weeks after inoculation of cells using calipers. Tumor volume was calculated by the formula $V = (a^2 \times b)/2$ (a is the width and b is the length in mm, respectively). Animal experiment was approved by the Institutional Ethics Committee on Animal Care and Experimentation at The Catholic University of Korea (approval number: 2016–035)

2.18. Immunohistological analysis of NRF2 and CD44 in breast cancer tissue array

To evaluate the expression of CD44 and NRF2 in normal and tumor breast tissues, commercially available tissue array slide containing 42 breast cancers and 21 corresponding normal tissues (ISU ABXIS, Seoul, Republic of Korea) was purchased. The double immunofluorescent staining was carried out using the previously established method [40]. Briefly, the silde was rehydrated following deparaffinization, and subjected to antigen retrieval by wet autoclaving at 120 °C for 5 min. After blocking with 5% FBS in PBS for 1 h at room temperature, the slide was incubated with primary antibodies for CD44 and NRF2 (ab62352, Abcam, Cambridge, MA, USA) in humidity chamber at 4 °C overnight. The section was incubated with Alexa fluor™ 488 goat anti-mouse IgG (a dilution at 1:1000) and then Alexa fluor™ 555 goat anti-rabbit IgG (a dilution at 1:1000) at a room temperature for 1 h. Finally, the section was mounted and counterstained with Vectashield™ mounting medium containing 4',6-diamidino-2-phenylindole (DAPI). All incubation steps were performed in a dark humidity chamber and the sections were rinsed in 0.01 M PBS 3-times between each step. As a negative control for Alexa fluor™ 488 and 555, the slide was incubated secondary antibodies without primary antibodies.

2.19. Histomorphometric analysis

Histological fields from the acinar-ductal and interstitial region of each sample were used for histomorphometrical analysis. CD44, NRF2, or CD44/NRF2-positive cells were identified under the fluorescent microscope (Eclipse 80i, Nikon, Tokyo, Japan), and the criterion for positive cells was that cells showed over 20% of immunofluorescent intensity when compared to the negative control. The mean numbers of CD44-, NRF2-, and CD44/NRF2-immunopositive cells were calculated using an automated image analyzer (iSolution FL ver 9.1, IMT i-solution Inc., Vancouver, Canada) and represented as cells/mm^2. The histopathologist was blinds to group distribution when this analysis was made. All histomorphometrical values are expressed as mean ± SE of histological fields from 42 breast cancer tissues or 21 normal tissues. For statistical analysis, the Mann-Whitney U (MW) test was conducted following the examination of variance homogeneity using the Levene test.

2.20. Statistical analysis

Statistical significance was analyzed using Student's *t*-test or a one-way analysis of variance (two-way ANOVA) followed by the Student Newman–Keuls test for multiple comparisons using Prism software (GraphPad Prism, La Jolla, CA, USA).

3. Results

3.1. CD44s is elevated in CSC-enriched MCF7/ADR cells

To investigate the potential relationship between anticancer drug resistance and CSCs, we used a doxorubicin-resistant MCF7 cell line (MCF7/ADR). These cells exhibited enhanced cell viability following incubation with doxorubicin for 72 h when compared to control MCF7 cells (Fig. 1A). In line with anticancer resistance, MCF7/ADR cells expressed higher levels of CSC markers, including SOX2, OCT4, and MDR1, than MCF7 cells (Fig. 1B). Notably, immunocytochemical analysis showed that the expression of the breast CSC marker CD44 was significantly high in MCF7/ADR than in MCF7 cells (Fig. 1C). Flow-cytometric analysis revealed that > 95% of MCF7/ADR cells were CD44-positive (CD44 +) cells, while < 5% MCF7 cells were CD44 + (Fig. 1D). Alternative splicing of *CD44* generates more than 20 known isoforms of CD44 protein [11,12]. To identify the CD44 isoform that is elevated in MCF/ADR, the expression of CD44 isoforms was assessed by RT-PCR analysis. The transcript level of total CD44 was higher in ADR than in MCF7 control cells, which was in accordance with the protein levels. Among all isoforms, the standard isoform CD44s showed substantially higher expression in ADR cells, whereas the transcript level of isoform 3 (CD44v3) was similar in both cell lines and that of CD44v8-10 was diminished in ADR cells (Fig. 1E). Western blot analysis confirmed the RT-PCR results: ADR cells showed a profound increase in CD44s (85–90 kDa) compared to MCF7 control cells (Fig. 1F). Collectively, these results indicated that the doxorubicin-resistant MCF7/ADR cells express high levels of CD44s along with CSC markers.

3.2. NRF2 signaling is activated in $CD44^{high}$ cancer-cell population

A number of studies have demonstrated that NRF2 contributes to chemoresistance in different types of cancer cells [27,28]. We investigated whether NRF2 signaling was activated in CSC-enriched MCF7/ADR cells. Transcript levels of the NRF2-target genes aldo-keto reductase 1C1 (*AKR1C1*), heme oxygenase-1 (*HO-1*), and glutamate cysteine ligase catalytic subunit (*GCLC*) were elevated by 3.8-, 1.9-, and 1.2-fold, respectively, in ADR cells (Fig. 2A). Immunoblot analysis NRF2 and AKR1C1 proteins were upregulated in ADR cells (Fig. 2B). However, transcript levels of *NRF2* did not show a significant difference between both cell lines (Fig. 2C). To investigate whether there is a direct link between NRF2 and CSCs, we isolated the CD44 + cell population ($CD44^{high}$) from MCF7/ADR cells using flow cytometry. $CD44^{high}$ cells exhibited stronger CD44s and NRF2 expression than the $CD44^{low}$

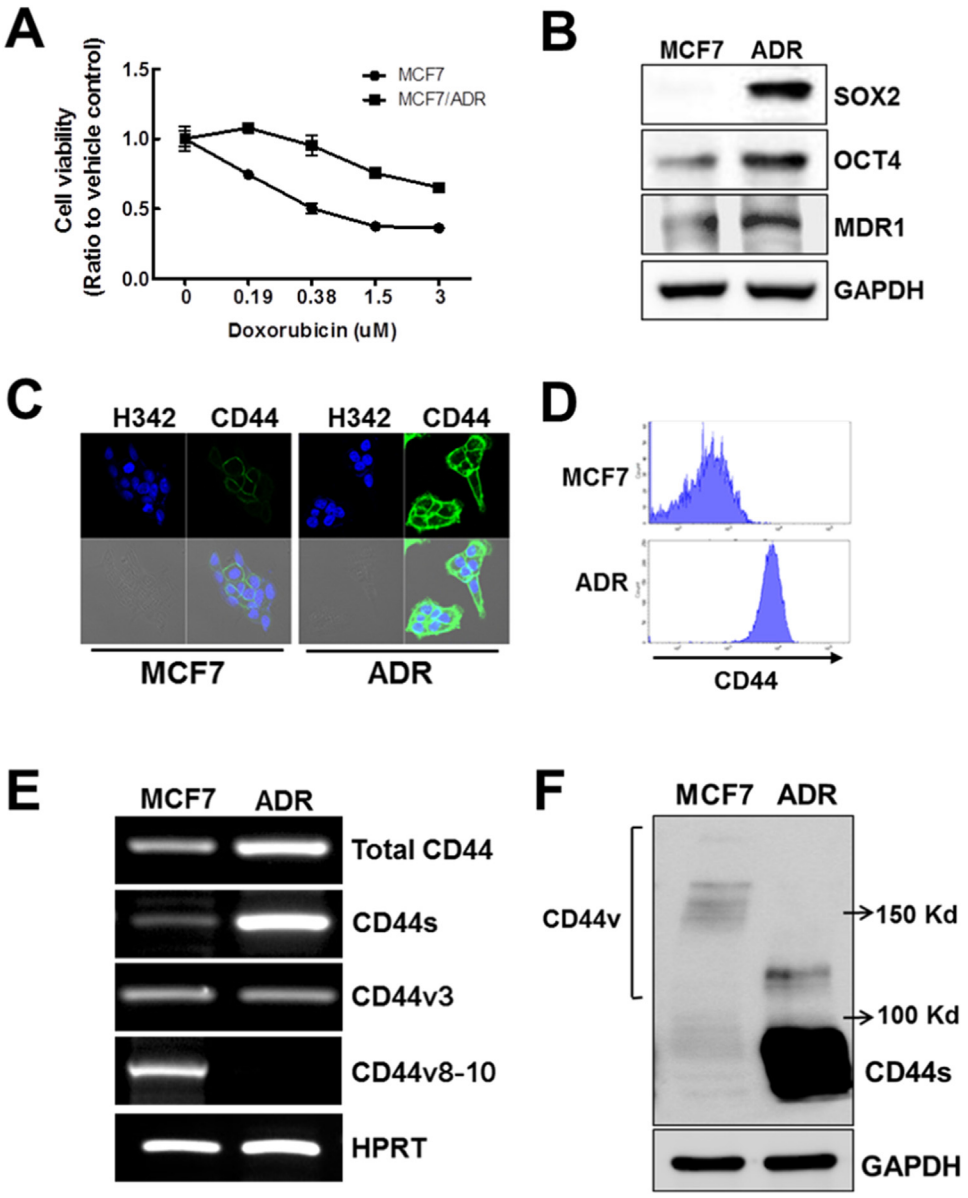

Fig. 1. CD44s is elevated in doxorubicin-resistant MCF7/ADR cells. (A) Cell viability was monitored after incubation with doxorubicin for 72 h in MCF7 and MCF7/ADR (ADR) cells. Values represent the mean ± SE from 6 sampled wells. (B) SOX2, OCT4, and MDR1 protein levels were determined in MCF7 and ADR cells using western blot analysis. (C) Immunocytochemical analysis of CD44 was carried out in MCF7 and ADR cells. (D) Total CD44 expression in MCF7 and ADR cells was determined using flow cytometry analysis (E) Transcript levels for total *CD44* and its isoforms (*CD44s*, *v3*, and *v8-10*) in ADR cells were assessed using RT-PCR analysis. (F) Protein levels of CD44 were determined in MCF7 and ADR cells using a CD44-reactive antibody. Similar blots were obtained in three independent experiments (B, E, and F).

population of ADR (Fig. 2D). These results indicated that NRF2 signaling was activated in CD44 + breast cancer stem-like cells.

To confirm the association of NRF2 with $CD44^{high}$, we isolated the $CD44^{high}$ population from normal MCF7 cells; we found a significant increase in NRF2 protein, along with enhanced AKR1C1 expression, as compared to the $CD44^{low}$ population from MCF7 (Fig. 2E). In addition, we confirmed NRF2 elevation in $CD44^{high}$ populations from breast cancer MDA-MB231 and lung cancer A549 (Fig. 2F and G). These results supported that there is a relation between NRF2 and CD44.

3.3. Establishment of a stable $CD44^{high}$ cell line, ADR44P

In an attempt to establish a CSC-like cell line, isolated $CD44^{high}$ cells were maintained in normal culture medium to establish a CSCs-like cell line system. The criterion for isolating $CD44^{high}$ cells was a cell-sorting of 50% of cells with strong CD44 staining from MCF7/ADR cells (Supplementary Fig. S1). At 16 days after isolation, $CD44^{high}$ cells exhibited their high CD44 expression property and the stable $CD44^{high}$ cell line (ADR44P) was obtained following one-month maintenance. In the stable CD44P cells, the CD44s level was substantially high, and most cells were CD44 + /CD24– (Fig. 3A). In addition, ADR44P cells expressed high levels of SOX2, OCT4, and MDR1, indicating enrichment of CSC-like breast cancer cells (Fig. 3B). As phenotypic characteristics, ADR44P cells showed stronger sphere formation, colony formation, and invasion capacities when compared to MCF7 (Fig. 3C-E). NRF2 expression remained elevated in CSC-like ADR44P cells. Total cellular NRF2 as well as cytosolic and nuclear NRF2 were elevated in ADR44P (Fig. 3F and G). Cytosolic and nuclear KEAP1 protein levels were not notably different between MCF7 and ADR44P (Fig. 3G). Taken together, these data displayed that the ADR44P cells established in the current study can be used as CSC-like cells, and that NRF2 signaling is activated in ADR44P cells.

3.4. NRF2 elevation is directly mediated by CD44s in ADR44P

To elucidate the link between CD44s and NRF2 expression, we silenced *CD44s* expression in ADR44P and examined changed in NRF2 expression. When ADR44P was transfected with *CD44* siRNA (siCD44), CD44 transcript level was reduced by 58% compared to the control RNA (siCN) transfection group (Supplementary Fig. S2). Immunoblot analysis revealed that the protein levels of CD44s, NRF2, and AKR1C1 were decreased by *CD44s* silencing and specifically, the NRF2 protein

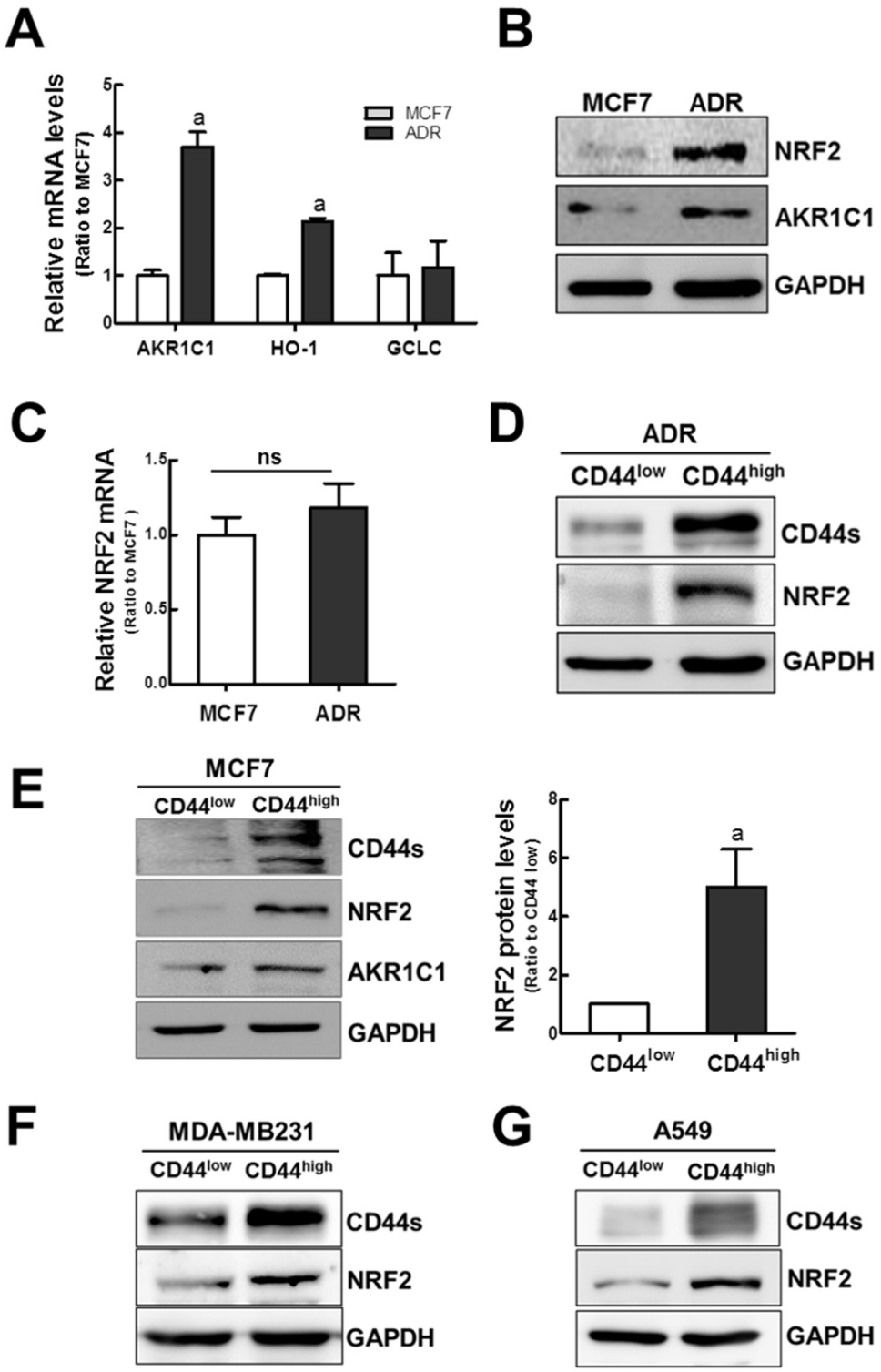

Fig. 2. NRF2 signaling is activated in MCF7/ADR cells. (A) Transcript levels for *AKR1c1*, *HO-1*, and *GCLC* were monitored in MCF7 and MCF7/ADR (ADR) cells using real-time RT-PCR analysis. Values represent the mean ± SE from 3 experiments. $^{a}P < 0.05$ compared with MCF7 cells. (B) Protein levels of total cellular NRF2 and AKR1C1 were determined in MCF7 and ADR cells using western blot analysis. (C) *NRF2* transcript levels were monitored in MCF7 and ADR cells. There was no significant difference (ns) between MCR7 and ADR cells. (D) Protein levels of CD44s and total NRF2 were determined in $CD44^{low}$ and $CD44^{high}$ cell populations isolated from MCF7/ADR cells. (E) Levels of CD44s, total NRF2, and AKR1C1 were assessed in $CD44^{low}$ and $CD44^{high}$ cell populations isolated from normal MCF7 cells. NRF2 levels were quantified and values represent the mean ± SE from 4 experiments. $^{a}P < 0.05$ compared with $CD44^{low}$ cells. (F-G) CD44s and total NRF2 protein levels were determined in $CD44^{low}$ and $CD44^{high}$ cell population isolated from MDA-MB231 (F) and A549 (G) cells using western blot analysis. Similar blots were obtained in three independent experiments (B, D, E, F, and G).

level was reduced by approximately 65% (Fig. 4A). There was no significant change in NRF2 mRNA expression following *CD44s* silencing (Fig. 4B). In line with the diminished NRF2 protein, the transcript levels of the NRF2 target genes *AKR1C1*, *HO-1*, and *GCLC* were significantly decreased by *CD44s* silencing (Fig. 4C). These results suggested that NRF2 elevation is directly mediated by CD44s.

Next, we elucidated the effect of CD44s overexpression on the NRF2 level. Forced expression of CD44s in MCF7 (MCF7-pCD44s) resulted in increased protein expression of NRF2 and AKR1C1 (Fig. 4D), and elevated mRNA expression of AKR1C1, HO-1, and GCLC as compared to the empty-plasmid control group (Fig. 4E).

The direct role of CD44 in NRF2 expression was further supported by the effect of the CD44 ligand hyaluronic acid. When ADR44P cells were incubated with hyaluronic acid (25 or 50 μg/mL), the levels of NRF2 and AKR1C1 increased in a concentration-dependent manner (Fig. 4F). Similarly, in MCF7-pCD44s cells, NRF2 and AKR1C1 expression was additionally increased following hyaluronic acid exposure (50 μg/mL) for 24 h (Fig. 4G). These findings clearly showed the CD44s-mediated NRF2 elevation in CSC-like breast cancer cells.

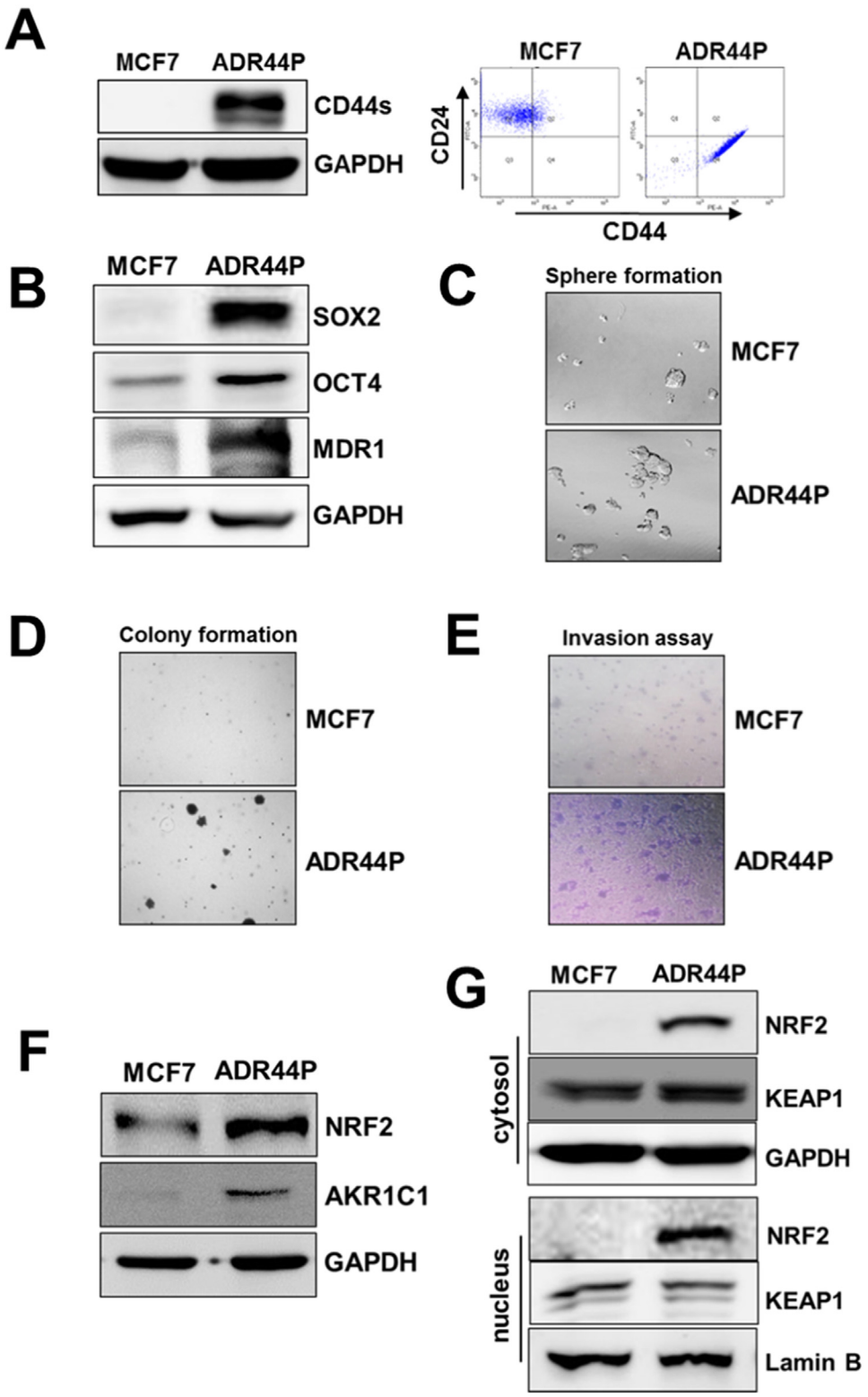

Fig. 3. Establishment of a CD44-positive CSC-like cell line and elevation of NRF2 in ADR44P. (A) CD44s protein levels were determined in ADR44P and MCF7 cells using western blotting. Cell population distribution was assessed in ADR44P and MCF7 cells following the incubation of cells with CD44 and CD24 antibodies. (B) Levels of SOX2, OCT4, and MDR1 were determined in ADR44P and MCF7. (C) Sphere formation capacity was assessed after 3 days of sphere culture of ADR44P and MCF7 cells. (D-E) Soft agar colony formation (D) and Transwell cell migration and invasion assays (E) were conducted using ADR44P and MCF7 cells. (F) Protein levels of total cellular NRF2 and AKR1C1 were detected in ADR44P and MCF7 cells. (G) Protein levels of cytosolic and nuclear NRF2 and KEAP1 were monitored in ADR44P and MCF7 using western blotting. Similar blots were obtained in three independent experiments (A, B, F, and G).

3.5. *p62 is involved in CD44s-mediated NRF2 activation*

Our previous study showed that NRF2 elevation was associated with 26S proteasome reduction and p62 elevation in CSC-enriched mammospheres [34]. On the basis of this finding, we aimed to elucidate the underlying molecular mechanisms of CD44s-mediated NRF2 elevation. First, we measured 26S proteasome expression, which revealed that the levels of proteasome catalytic subunits PSMB5, PSMB6, and PSMB7 were not changed in ADR44P cells (Supplementary Fig. S3). Second, we assessed potential p62 involvement in NRF2 activation in ADR44P cells. Transcripts as well as protein levels of p62 were significantly higher in ADR44P than in control MCF7 cells (Fig. 5A and B). Silencing of *CD44s* in ADR44P cells repressed the p62 level, indicating that elevated p62 level is mediated by CD44s (Fig. 5C), whereas forced expression of CD44s in MCF7 increased p62 expression (Fig. 5D). Finally, *p62* silencing in ADR44P cells reduced the expression of NRF2 and its target

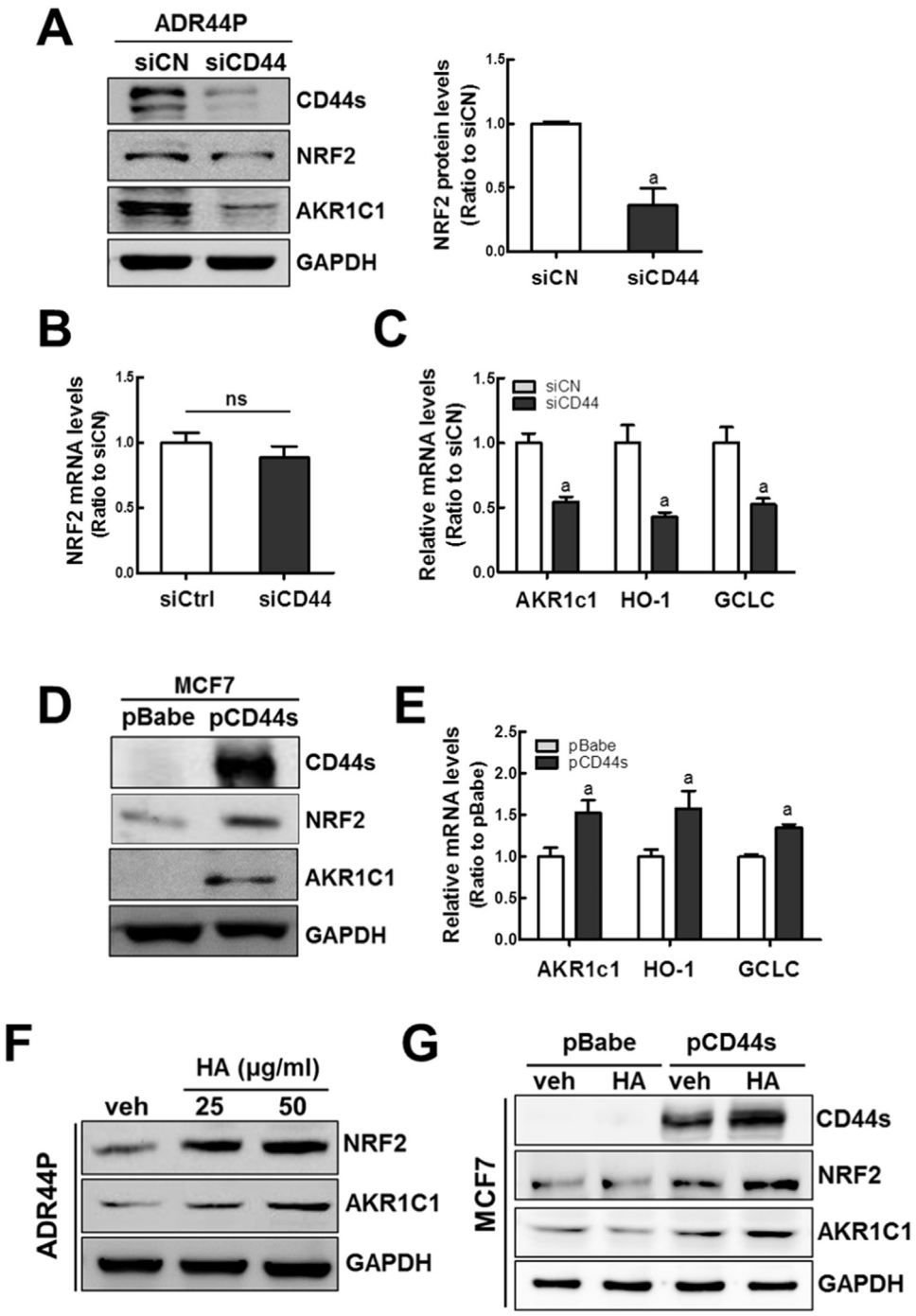

Fig. 4. CD44s is involved in NRF2 activation. (A) CD44-specific siRNA (siCD44) or non-specific control RNA (siCN) was transfected into ADR44P cells, and protein levels of CD44s, NRF2, and AKR1C1 were determined. Values represent the mean ± SE from 3 experiments. [a]P < 0.05 compared with siCN cells. (B) Transcript levels of *NRF2* were monitored in siCD44 and siCN cells using real-time PCR analysis. (C) Transcript levels of *AKR1C1*, *HO-1*, and *GCLC* were assessed in siCD44 and siCN cells. Values represent the mean ± SE from 3 experiments. [a]P < 0.05 compared with siCN cells. (D) CD44s expression plasmid (pBabe-CD44s) or blank plasmid (pBabe) was transfected into MCF7 cells, and stable cell lines (pCD44s and pBabe) were established. Protein levels of CD44s, NRF2, and AKR1C1 were measured in pCD44s and pBabe cells. (E) Transcript levels for *AKR1C1*, *HO-1*, and *GCLC* were assessed in pCD44s and pBabe cells using real-time PCR analysis. Values represent the mean ± SE from 3 experiments. [a]P < 0.05 compared with the pBabe control cells. (F) ADR44P cells were incubated with hyaluronic acid (HA, 25 and 50 μg/mL) for 24 h, and levels of NRF2 and AKR1C1 were monitored. (G) pBabe and pCD44s cells were incubated with HA (50 μg/mL) for 24 h, and protein levels of CD44s, NRF2, and AKR1C1 were monitored using western blotting. Similar blots were obtained in three independent experiments (A, D, F, and G).

genes (Supplementary Fig. S4, Fig. 5E, and F). However, CD44s expression was not affected by p62 silencing (Fig. 5G). It remains unclear by which mechanism CD44s led to p62 elevation; however, based on reports showing the activation of autophagy in CSCs, altered autophagy may cause p62 elevation in ADR44P cells. Indeed, the autophagy marker LC3-II was elevated in ADR44P cells (Fig. 5H), and ADR44P had more autophagic vacuoles than MCF7 cells (Fig. 5I). These results suggested that the $CD44^{high}$ CSC-like cells activate the autophagy response, leading to p62 elevation, which is a mediator in NRF2 activation.

3.6. Role of NRF2 in CSC-like properties of ADR44P

Our results showed that the $CD44^{high}$ CSC-like cells strongly express NRF2. This raised the question whether NRF2 elevation contributes to the CSC phenotype of ADR44P. To answer this question, we investigated the effects of NRF2 inhibition on phenotypic characteristics of CSC-like cells. Transient silencing of *NRF2* in ADR44P cells (siNRF2) resulted in a 60% reduction in *NRF2* transcript levels (Supplementary Fig. S5), and suppressed the protein expression of NRF2 and AKR1C1 (Fig. 6A). CD44s expression was not affected by *NRF2* silencing, which confirms that CD44s mediates the enhanced NRF2 expression. The levels of CSC markers SOX2 and OCT4 were not diminished by *NRF2* silencing (Fig. 6B). As a result of reduced NRF2 target gene expression, intracellular ROS levels in shNRF2 cells were higher than those in control cells (Fig. 6C). As a phenotypic effect, stable silencing of *NRF2* (shNRF2; Supplementary Fig. S6) resulted in the inhibition of sphere formation of ADR44P (Fig. 6D). The average diameters of control

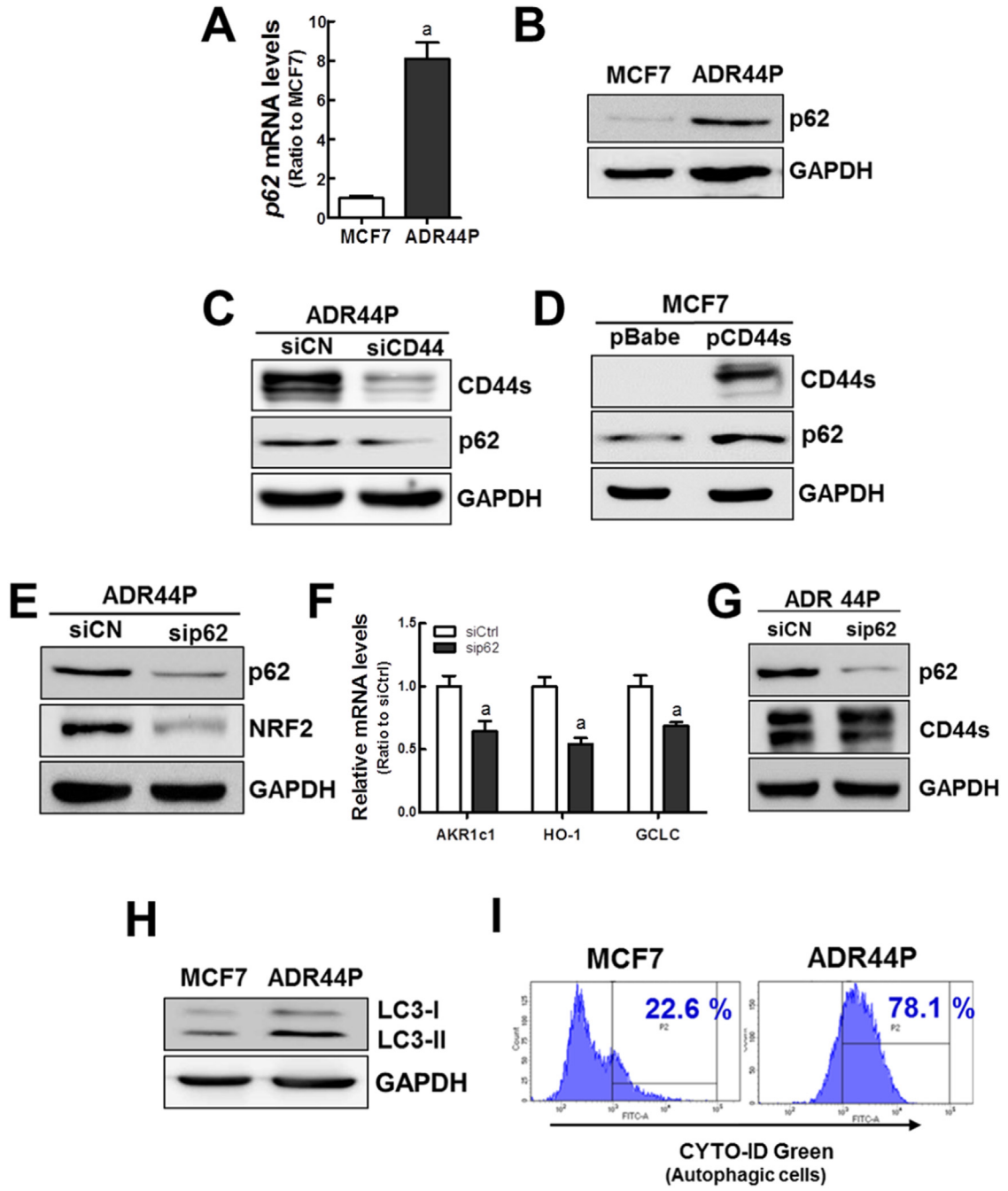

Fig. 5. p62 is involved in CD44s-mediated NRF2 activation. (A) Transcript levels for *p62* were measured in ADR44P and MCF7 cells using real-time PCR analysis. Values represent the mean ± SE from 3 experiments. $^{a}P < 0.05$ compared with the control MCF7. (B) p62 protein levels were determined in ADR44P and MCF7. (C) ADR44P cells were transfected with CD44-specific siRNA (siCD44) or control siRNA (siCN), and p62 protein levels were determined using western blotting. (D) MCF7 cells were transfected with pBabe-CD44s or blank plasmid pBabe, and levels of CD44s and p62 were monitored in these stable cell lines. (E) ADR44P cells were transfected with p62-specific siRNA (sip62) or control siRNA (siCN), and levels of p62 and NRF2 were determined in siCN and sip62 cells. (F) Transcript levels of *AKR1C1*, *HO-1*, and *GCLC* were relatively quantified in sip62 and siCN cells.(G) Levels for CD44s were determined in sip62 and siCN cells. (H) Levels of LC3 (LC3-I and LC3-II) were determined in ADR44P and MCF7 using western blotting. (I) ADR44P and MCF7 cells were incubated with the Cyto-ID autophagy detection reagent, and green fluorescence from autophagic vacuoles was measured by flow cytometry (488 nm). Similar blots were obtained in three independent experiments (B, C, D, F, and H).

spheres and shNRF2 spheres were 67 μm and 48 μm, respectively. *NRF2* silencing suppressed the colony formation and invasion capacities of ADR44P (Fig. 6E and F). Additionally, an MTT assay showed that the *NRF2*-silenced ADR44P cells displayed more cell death following 72-h incubation with doxorubicin or daunorubicin than the sc control cells (Fig. 6G and H). These data suggested that NRF2 plays crucial roles in the acquisition of an aggressive phenotype and chemoresistance in $CD44^{high}$ CSC-like cells.

3.7. NRF2-silenced ADR44P cells show retarded tumor growth

To examine whether NRF2 can affect ADR44P tumorigenicity, we performed a tumor xenograft assay. To compare tumorigenic potential of the sc control and shNRF2-ADR44P cells, these cells were inoculated

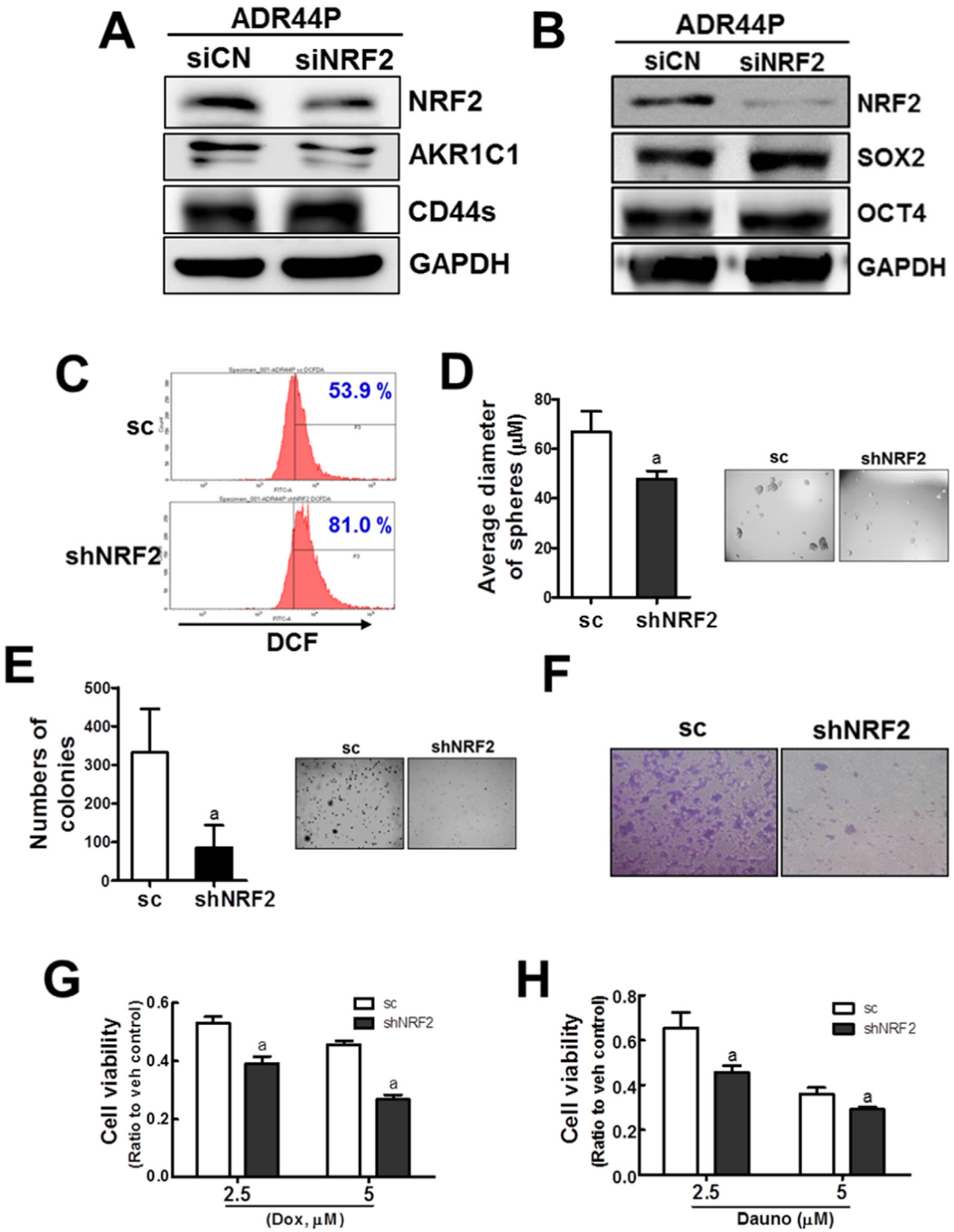

Fig. 6. Drug resistance and aggressive phenotype of ADR44P are diminished by *NRF2* knockdown. (A) NRF2-specific siRNA (siNRF2) or control siRNA (siCN) was introduced into ADR44P cells, and levels of NRF2, AKR1C1, and CD44s were determined. (B) Levels of SOX2 and OCT4 were measured in siNRF2 and siCN transfected ADR44P cells. (C) Levels of intracellular ROS were assessed in siNRF2- and siCN-transfected ADR44P cells following incubation of the cells with DCFDA. Cell population with fluorescence was monitored by flow cytometry. (D) Stable cell lines (shNRF2- and sc-ADR44P) were established following transduction of ADR44P cells with NRF2 shRNA- or non-specific scrambled (sc) RNA-containing lentiviral particles. Sphere formation was assessed in shNRF2 and sc-ADR44P cells following 3 days of sphere culture. Average sphere diameters were determined using the image processing software ToupView. Values represent the mean ± SE from 3 to 4 sampled wells. $^{a}P < 0.05$ compared to the sc control group. (E) Soft agar colony formation was assessed in shNRF2 and sc-ADR44P cells. Colony number was quantified. Values represent the mean ± SE from 3 dishes. $^{a}P < 0.05$ compared to the sc control group. (F) Transwell cell migration and invasion assays were carried out using shNRF2 and sc-ADR44P cells. (G-H) Viability of shNRF2 and sc-ADR44P cells was monitored following exposure to doxorubicin (G; 2.5 and 5 μM) or daunorubicin (H; 2.5 and 5 μM) for 72 h. Values represent the mean ± SE from 8 sampled wells. $^{a}P < 0.05$ compared with sc control. Similar blots were obtained in three independent experiments (A and B).

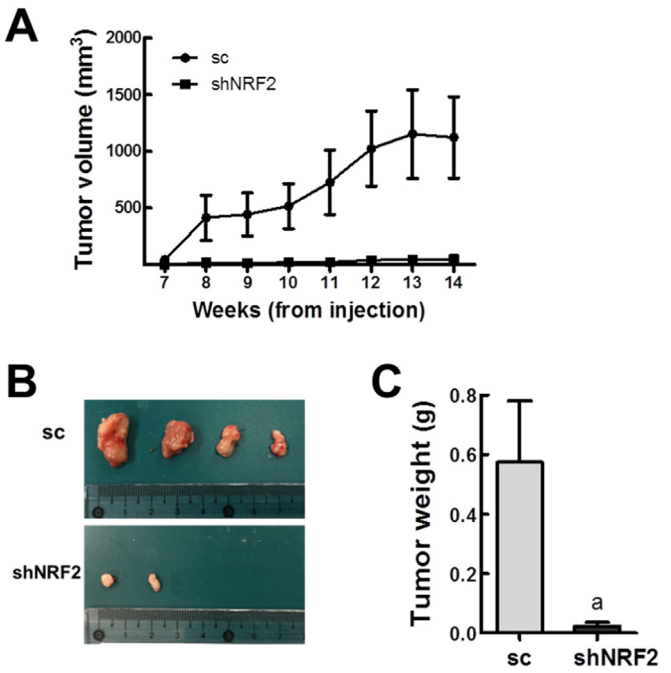

Fig. 7. *NRF2* knockdown results in suppression of tumor growth of ADR44P. (A) shNRF2 and sc-ADR44P cells were implanted in nude mice and tumor volume was measured every week from 7 to 14 weeks after inoculation. Tumor volume was calculated by the formula $V = (a^2 \times b)/2$ (a is the width and b the length in mm). $^{a}P < 0.05$ compared to the sc-ADR44P control. (B) Solid tumors were obtained from mouse xenografts of shNRF2 and sc-ADR44P cells. (C) shNRF2 and sc-ADR44P tumors were weighed at 14 weeks after inoculation. Values represent the mean ± SE from four animals. $^{a}P < 0.05$ compared to the sc-ADR44P control.

in nude mice. Seven weeks after cell inoculation, tumor growth of the sc control ADR44P cells continued and tumor volume reached up to 1100 mm^3 in the last week of observation. However, shNRF2-ADR44P cells showed substantially suppressed tumor growth (Fig. 7A and B). The average weight of shNRF2 tumors was significantly lower than that in the control group (Fig. 7C). These results indicated that NRF2 inhibition in CSC-like ADR44P cells can suppress tumor growth in mouse xenografts.

3.8. CD44 and NRF2 are upregulated and colocalize in breast tumor samples

In an attempt to obtain clinical evidence of the link between CD44 and NRF2, we carried out dual immunohistological analysis of CD44 and NRF2 using a tumor tissue array. The tissue array slide contained 42 breast cancers and 21 corresponding normal tissues. The results indicated CD44 and NRF2 were expressed on the cell surface and in the cytoplasm, respectively. Histomorphometric analysis of fluorescence intensities for CD44, NRF2, and CD44/NRF2 (colocalization) showed significant increases in CD44-, NRF2-, and CD44/NRF2-immunoreactive cells in both acinar-ductal and interstitial regions of breast cancer tissues when compared to those in corresponding normal tissues (Table 1 and Fig. 8A). Specifically, CD44 levels were elevated by 70-fold and 15-fold in acinar-ductal and interstitial regions of breast tumor samples, respectively, as compared to the corresponding regions in non-tumor samples (Table 1). NRF2 levels in the acinar-ductal and interstitial regions were 29-fold and 5-fold higher than those in non-tumor samples, respectively. Of note, 87.8% of acinar-ductal CD44 + tumor cells showed NRF2 expression as indicated by colocalization. Similarly, 73.3% of interstitial CD44 + tumor cells expressed high levels of NRF2 (Fig. 8B). These results supported our finding in vitro that CD44-positive cancer cells express high levels of NRF2.

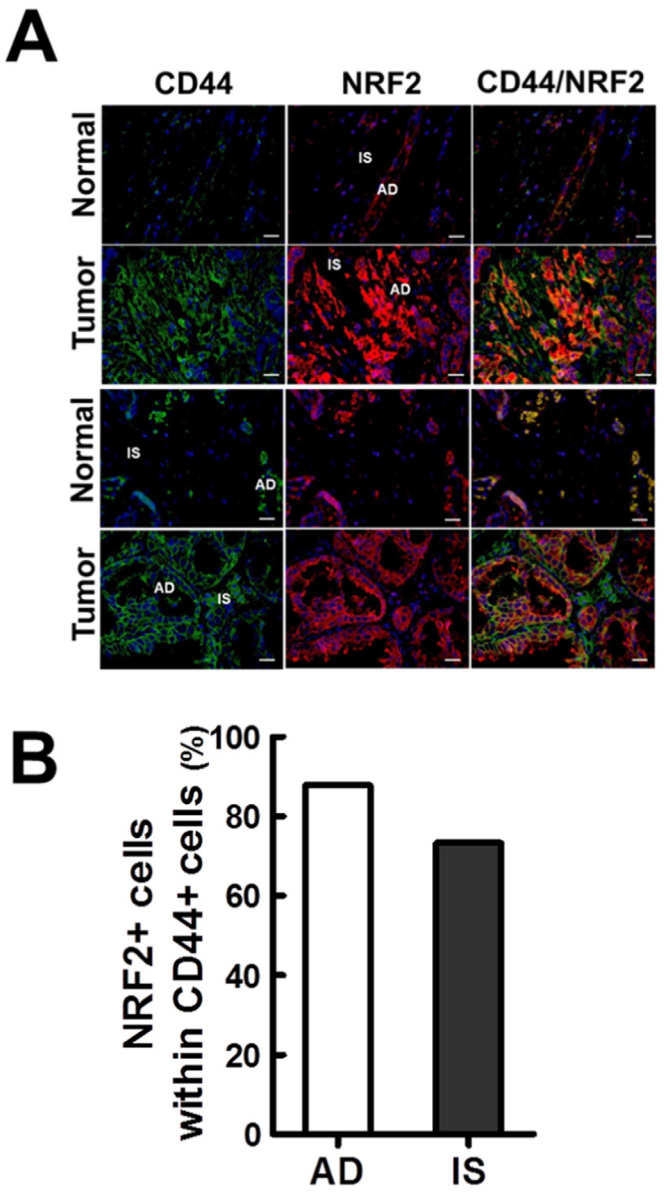

Fig. 8. CD44 and NRF2 are upregulated and colocalize in breast tumor samples. (A) Representative fluorescence profiles for CD44, NRF2, and CD44/NRF2 colocalization in two pairs of breast tumors and corresponding normal tissues. AD, acinar-ductal region; IS, interstitial region. Scale bars = 20 μm. (B) Percentage of NRF2-positive cells within CD44-positive acinar-ductal (AD) and interstitial (IS) regions of breast tumor samples.

4. Discussion

CD44 is the most common CSC marker in various types of cancer, including breast cancer [11,12]. The potential contribution of CD44 to ROS metabolism has gained increasing attention because of the critical role of ROS in stem cell maintenance and survival. As the ROS level is associated with the regulation of the proliferation and self-renewal capacities of stem cells, some CSCs maintain higher levels of ROS-metabolizing enzymes than normal cells, similar to adult stem cells [5–7]. The $CD44^{high}CD24^{low}$ CSCs from breast tumors exhibited higher expression of GPX, SOD, and catalase and are more resistant to ROS-induced cell death than normal cells [7]. As a molecular mechanism of differential antioxidant capacity and stress resistance of CSCs, the current study identified a direct association of CD44s with NRF2 signaling. We observed that the NRF2 protein level was elevated in $CD44^{high}$ subpopulations from breast cancer cell lines MCF7, MCF7/

Table 1
Histomorphometric analysis of double immunofluorescence staining of CD44 and NRF2. NRF2-, CD44-, and NRF2/CD44-positive cells in the acinar-ductal and interstitial regions of breast cancer and normal tissues.

Regions (Unit) Groups	Acinar-ductal (cells/mm^2)			Interstitial (cells/mm^2)		
	NRF2	CD44	NRF2/CD44	NRF2	CD44	NRF2/CD44
Normal tissue	11.81 ± 8.49	3.05 ± 2.12	0.57 ± 0.42	64.38 ± 12.18	17.71 ± 3.08	12.95 ± 2.15
Breast cancer	339.05 ± 41.72[a]	213.52 ± 35.96[a]	187.43 ± 31.18[a]	340.38 ± 48.95[a]	267.14 ± 45.04[a]	195.90 ± 35.44[a]

Values are expressed as the mean ± SE of 42 breast cancer and 21 corresponding normal tissue spots.
[a] $p < 0.01$ as compared with normal tissue spots by MW test.

ADR, and MDA-MB231, and lung cancer cell line A549, when compared to CD44^{low} subpopulations. We demonstrated that NRF2 elevation was mediated thorugh CD44s-p62 signaling, and high NRF2 level contributed to the maintenance of low ROS and development of CSC-like peorperties of in CD44^{high}CD24^{low} breast cancer cells, including drug resistance, colony/sphere formation, cell migration, and facilitated tumor growth. These results provide molecular insights into the CD44-induced CSC phenotype by demonstrating NRF2 activation and its role in CSC-like properties. Considering the high levels of hyaluronic acid in tumor stroma [41], it is highly likely that the hyaluronic acid/CD44s-mediated NRF2 activation could be the programmed mechanism of protection against the ROS-rich tumor microenvironment in CSCs. It should be noted that CD44v is also involved in ROS protection. A study by Ishimoto *et al.* demonstrated that CD44v8-10 stabilizes xCT, a light-chain subunit of the cysteine-glutamate transporter, through direct interaction and consequently upregulates GSH synthesis in human gastrointestinal cancer cells [42]. Although CD44 isoforms have different molecular mechanisms, CD44 might be a common linker molecule that provides CSCs with ROS defense capacity and stress resistance.

The involvement of NRF2 in CSC resistance has been suggested by several previous studies. In a study by Achuthan *et al.*, drug-resistant breast cancer cells displayed a CSC-like phenotype, including high CD133 and OCT4 expression, and these cells expressed high levels of NRF2, SOD, and GPXs [43]. Proteomic analysis revealed that NRF2-regulated antioxidant and detoxifying proteins were highly enriched in the CSCs-derived secretome [44]. *NRF2* knockdown attenuated tumorigenicity in glioblastoma stem cells [45], and *NRF2*-inhibited mammospheres showed decreased cell proliferation and chemoresistance [32]. The high NRF2 level in spheroids of breast and colon cancer cells was associated with enhanced expression of drug efflux transporters and consequent drug resistance [33,34]. In line with these reports, the current study provides evidence that the NRF2 level is upregulated in CD44^{high} breast CSC-like cells, which eventually contributes to the CSC phenotype and drug resistance. As supportive evidence, several reports have suggested possible correlations between CD44 and NRF2. A study by Kim *et al.* showed that the expression of NRF2 as well as its target genes were relatively high in the CD4$^+$/CD44^{high} subset of memory T cells when compared to the CD4$^+$/CD44^{low} subset [46]. Immunohistological analysis of hepatitis C virus-associated hepatocellular carcinoma revealed strongly increased NRF2 expression in CD44v9$^+$ cancer cells, and this positive expression was significantly associated with poor prognosis for recurrence-free survival [47].

In addition to its role in the autophagic process, p62 exerts various cellular functions by interacting with multiple signaling molecules, including NRF2 [22,48]. In particular, recent findings highlightes aberrant p62 overexpression and its implication in tumor progression. In breast cancer patients, high p62 expression was associated with advanced clinical stages and correlates with a higher degree of tumor invasion [49]. In hepatocellular carcinoma, p62 accumulation accelerated tumor development via elevation of antioxidant proteins [50]. In this study, p62 was identified as a molecular link between CD44 and NRF2 activation in breast CSC-like cells. The transcript and protein levels of p62 were increased in the CD44^{high}CD24^{low} ADR44P as well as MCF7 overexpressing CD44s, and *p62* silencing abolished NRF2 accumulation. These results indicate the critical role of p62 in CSC properties of CD44^{high} CSCs via NRF2 elevation. In addition to CD44^{high}-enriched CSC system, p62 elevation was responsible for NRF2 accumulation in spheroid CSC-like cells [34]. Recently, a report by Xu *et al.* elucidated that p62 elevation is a common molecular event in different types of CSC systems [51]. Breast CSC systems, including mammospheres, the CD44^{high}CD24^{low} subpopulation, the aldehyde dehydrogenase (ALDH) 1A1-positive subpopulation, and the side population, maintained high levels of p62, and this elevation was closely relevant to stem-like properties and facilitated tumor growth of breast CSCs. Although this study demonstrated that high expression of stemness-associated genes was a results of the p62-mediated *MYC* mRNA stabilization, p62 activation might be a core molecular event in CSCs for survival.

It is currently not clear how p62 was elevated in CSC-like cells; however, the autophagic alteration in CSCs might be a cause of p62 elevation. The levels of the autophagy molecule Beclin 1 and autophagic flux were high in the ALDH1A1^{high} subpopulation from breast spheroids when compared to ALDH^{low} cells [52]. CD44^{high} colorectal CSCs displayed autophagy activation, and enhanced autophagy was involved in chemoresistance to paclitaxel [53]. The ADR44P cells established here showed increases in the autophagy marker LC3B-II and autophagic flux levels when compared to CD44^{low} cells, indicating autophagy activation. These suggest that autophagy activation might be an essential cellular process for CSC adaption and survival. Indeed, it should be noted that CSC would favor catabolic metabolism because CSCs are located in tumor environment with nutrient depletion and hypoxia [54]. How the increase in autophagy leads to an increase in p62 remains to be examined in future.

Taken together, our data indicated that CD44s expression led to p62-associated NRF2 activation in CD44^{high} breast CSC-like cells. High NRF2 in CD44^{high} CSC-like cells contributed to the aggressive CSC phenotypes, including enhanced sphere/colony formation and invasion, facilitated tumor growth, and anticancer drug resistance. Therefore, the CD44-NRF2 axis might be an effective therapeutic target for the control of stress resistance and survival of the CD44^{high} CSC population.

Source of funding

This study was financially supported by a grant from the National Research Foundation of Korea (NRF) funded by the Korea government (MSIP) (NRF-2015R1A2A1A10054384). This study was also supported by the BK21Plus grant of NRF funded by Korean government (22A20130012250).

Disclosure

None.

Conflict of interest

The authors declare that they have no conflict of interest.

Appendix A. Supplementary material

Supplementary data associated with this article can be found in the online version at http://dx.doi.org/10.1016/j.redox.2018.04.015.

References

[1] D. Bonnet, J.E. Dick, Human acute myeloid leukemia is organized as a hierarchy that originates from a primitive hematopoietic cell, Nat. Med. 3 (1997) 730–737.
[2] S.K. Singh, C. Hawkins, I.D. Clarke, J.A. Squire, J. Bayani, T. Hide, et al., Identification of human brain tumour initiating cells, Nature 432 (2004) 396–401.
[3] M. Al-Hajj, M.S. Wicha, A. Benito-Hernandez, S.J. Morrison, M.F. Clarke, Prospective identification of tumorigenic breast cancer cells, Proc. Natl. Acad. Sci. USA 100 (2003) 3983–3988.
[4] A. Eramo, F. Lotti, G. Sette, E. Pilozzi, M. Biffoni, A. Di Virgilio, et al., Identification and expansion of the tumorigenic lung cancer stem cell population, Cell Death Differ. 15 (2008) 504–514.
[5] K. Ito, A. Hirao, F. Arai, S. Matsuoka, K. Takubo, I. Hamaguchi, et al., Regulation of oxidative stress by ATM is required for self-renewal of haematopoietic stem cells, Nature 431 (2004) 997–1002.
[6] K. Ito, A. Hirao, F. Arai, K. Takubo, S. Matsuoka, K. Miyamoto, et al., Reactive oxygen species act through p38 MAPK to limit the lifespan of hematopoietic stem cells, Nat. Med. 12 (2006) 446–451.
[7] M. Diehn, R.W. Cho, N.A. Lobo, T. Kalisky, M.J. Dorie, A.N. Kulp, et al., Association of reactive oxygen species levels and radioresistance in cancer stem cells, Nature 458 (2009) 780–783.
[8] A.A. Dayem, H.-Y. Choi, J.-H. Kim, S.-G. Cho, Role of oxidative stress in stem, cancer, and cancer stem cells, Cancers 2 (2010) 859–884.
[9] E.D. Lagadinou, A. Sach, K. Callahan, R.M. Rossi, S.J. Neering, M. Minhajuddin, et al., BCL-2 inhibition targets oxidative phosphorylation and selectively eradicates quiescent human leukemia stem cells, Cell Stem Cell 12 (2013) 329–341.
[10] C.W. Chang, Y.S. Chen, S.H. Chou, C.L. Han, Y.J. Chen, C.C. Yang, et al., Distinct subpopulations of head and neck cancer cells with different levels of intracellular reactive oxygen species exhibit diverse stemness, proliferation, and chemosensitivity, Cancer Res. 74 (2014) 6291–6305.
[11] Y. Yan, X. Zuo, D. Wei, Concise review: emerging role of CD44 in cancer stem cells: a promising biomarker and therapeutic target, Stem Cells Transl. Med. 4 (2015) 1033–1043.
[12] M. Zöller, CD44: can a cancer-initiating cell profit from an abundantly expressed molecule? Nat. Rev. Cancer 11 (2011) 254–267.
[13] S. Tsukita, K. Oishi, N. Sato, J. Sagara, A. Kawai, S. Tsukita, ERM family members as molecular linkers between the cell surface glycoprotein CD44 and actin-based cytoskeletons, J. Cell Biol. 126 (1994) 391–401.
[14] L. Du, H. Wang, L. He, J. Zhang, B. Ni, X. Wang, et al., CD44 is of functional importance for colorectal cancer stem cells, Clin. Cancer Res. 14 (2008) 6751–6760.
[15] S. Takaishi, T. Okumura, S. Tu, S.S. Wang, W. Shibata, R. Vigneshwaran, et al., Identification of gastric cancer stem cells using the cell surface marker CD44, Stem Cells 27 (2009) 1006–1020.
[16] L. Patrawala, T. Calhoun, R. Schneider-Broussard, H. Li, B. Bhatia, S. Tang, et al., Highly purified CD44+ prostate cancer cells from xenograft human tumors are enriched in tumorigenic and metastatic progenitor cells, Oncogene 25 (2006) 1696–1708.
[17] C. Yoon, D.J. Park, B. Schmidt, N.J. Thomas, H.-J. Lee, T.S. Kim, et al., CD44 expression denotes a subpopulation of gastric cancer cells in which Hedgehog signaling promotes chemotherapy resistance, Clin. Cancer Res. 20 (2014) 3974–3988.
[18] J.D. Hayes, A.T. Dinkova-Kostova, The Nrf2 regulatory network provides an interface between redox and intermediary metabolism, Trends Biochem. Sci. 39 (2014) 199–218.
[19] K. Taguchi, M. Yamamoto, The KEAP1–NRF2 system in cancer, Front. Oncol. 7 (2017) 85.
[20] K. Itoh, N. Wakabayashi, Y. Katoh, T. Ishii, T. O'connor, M. Yamamoto, Keap1 regulates both cytoplasmic-nuclear shuttling and degradation of Nrf2 in response to electrophiles, Genes Cells 8 (2003) 379–391.
[21] H. Motohashi, M. Yamamoto, Nrf2–Keap1 defines a physiologically important stress response mechanism, Trends Mol. Med. 10 (2004) 549–557.
[22] A. Jain, T. Lamark, E. Sjøttem, K.B. Larsen, J.A. Awuh, A. Øvervatn, et al., p62/SQSTM1 is a target gene for transcription factor NRF2 and creates a positive feedback loop by inducing antioxidant response element-driven gene transcription, J. Biol. Chem. 285 (2010) 22576–22591.
[23] A. Lau, X.-J. Wang, F. Zhao, N.F. Villeneuve, T. Wu, T. Jiang, et al., A noncanonical mechanism of Nrf2 activation by autophagy deficiency: direct interaction between Keap1 andp62, Mol. Cell. Biol. 30 (2010) 3275–3285.
[24] K. Taguchi, N. Fujikawa, M. Komatsu, T. Ishii, M. Unno, T. Akaike, et al., Keap1 degradation by autophagy for the maintenance of redox homeostasis, Proc. Natl. Acad. Sci. USA 109 (2012) 13561–13566.
[25] M.J. Calkins, D.A. Johnson, J.A. Townsend, M.R. Vargas, J.A. Dowell, T.P. Williamson, et al., The Nrf2/ARE pathway as a potential therapeutic target in neurodegenerative disease, Antioxid. Redox Signal. 11 (2009) 497–508.
[26] H.-Y. Cho, S.P. Reddy, S.R. Kleeberger, Nrf2 defends the lung from oxidative stress, Antioxid. Redox Signal. 8 (2006) 76–87.
[27] A. Singh, H. Wu, P. Zhang, C. Happel, J. Ma, S. Biswal, Expression of ABCG2 (BCRP) is regulated by Nrf2 in cancer cells that confers side population and chemoresistance phenotype, Mol. Cancer Ther. 9 (2010) 2365–2376.
[28] X.-J. Wang, Z. Sun, N.F. Villeneuve, S. Zhang, F. Zhao, Y. Li, et al., Nrf2 enhances resistance of cancer cells to chemotherapeutic drugs, the dark side of Nrf2, Carcinogenesis 29 (2008) 1235–1243.
[29] B.-h. Choi, I.-g. Ryoo, H.C. Kang, M.-K. Kwak, The sensitivity of cancer cells to pheophorbide a-based photodynamic therapy is enhanced by Nrf2 silencing, PLoS One 9 (2014) e107158.
[30] T.-H. Kim, E.-g. Hur, S.-J. Kang, J.-A. Kim, D. Thapa, Y.M. Lee, et al., NRF2 blockade suppresses colon tumor angiogenesis by inhibiting hypoxia-induced activation of HIF-1α, Cancer Res. 71 (2011) 2260–2275.
[31] S. Manandhar, B.-h. Choi, K.-A. Jung, I.-g. Ryoo, M. Song, S.J. Kang, et al., NRF2 inhibition represses ErbB2 signaling in ovarian carcinoma cells: implications for tumor growth retardation and docetaxel sensitivity, Free Radic. Biol. Med. 52 (2012) 1773–1785.
[32] T. Wu, B.G. Harder, P.K. Wong, J.E. Lang, D.D. Zhang, Oxidative stress, mammospheres and Nrf2–new implication for breast cancer therapy? Mol. Carcinog. 54 (2015) 1494–1502.
[33] I.-g. Ryoo, G. Kim, B.-h. Choi, S.-h. Lee, M.-K. Kwak, Involvement of NRF2 Signaling in Doxorubicin Resistance of Cancer Stem Cell-Enriched Colonospheres, Biomol. Ther. 24 (2016) 482.
[34] I. Ryoo, B. Choi, M. Kwak, Activation of NRF2 by p62 and proteasome reduction in sphere-forming breast carcinoma cells, Oncotarget (2015).
[35] S. Manandhar, S. Lee, M.-K. Kwak, Effect of stable inhibition of NRF2 on doxorubicin sensitivity in human ovarian carcinoma OV90 cells, Arch. Pharmacal Res. 33 (2010) 717–726.
[36] K.-A. Jung, B.-h. Choi, C.-W. Nam, M. Song, S.-T. Kim, J.Y. Lee, et al., Identification of aldo-keto reductases as NRF2-target marker genes in human cells, Toxicol. Lett. 218 (2013) 39–49.
[37] M.-g. Song, I.-g. Ryoo, H.-y. Choi, B.-h. Choi, S.-T. Kim, T.-H. Heo, et al., NRF2 signaling negatively regulates phorbol-12-myristate-13-acetate (PMA)-induced differentiation of human monocytic U937 cells into pro-inflammatory macrophages, PLoS One 10 (2015) e0134235.
[38] S. Borowicz, M. Van Scoyk, S. Avasarala, M.K.K. Rathinam, J. Tauler, R.K. Bikkavilli, et al., The soft agar colony formation assay, J. Vis. Exp.: JoVE (2014).
[39] C.R. Justus, N. Leffler, M. Ruiz-Echevarria, L.V. Yang, In vitro cell migration and invasion assays, J. Vis. Exp.: JoVE (2014).
[40] P.-L. Lin, J.T. Chang, D.-W. Wu, C.-C. Huang, H. Lee, Cytoplasmic localization of Nrf2 promotes colorectal cancer with more aggressive tumors via upregulation of PSMD4, Free Radic. Biol. Med. 95 (2016) 121–132.
[41] E. Karousou, S. Misra, S. Ghatak, K. Dobra, M. Gotte, D. Vigetti, et al., Roles and targeting of the HAS/hyaluronan/CD44 molecular system in cancer, Matrix Biol. : J. Int. Soc. Matrix Biol. 59 (2017) 3–22.
[42] T. Ishimoto, O. Nagano, T. Yae, M. Tamada, T. Motohara, H. Oshima, et al., CD44 variant regulates redox status in cancer cells by stabilizing the xCT subunit of system xc(-) and thereby promotes tumor growth, Cancer Cell 19 (2011) 387–400.
[43] S. Achuthan, T.R. Santhoshkumar, J. Prabhakar, S.A. Nair, M.R. Pillai, Drug-induced senescence generates chemoresistant stemlike cells with low reactive oxygen species, J. Biol. Chem. 286 (2011) 37813–37829.
[44] B.L. Emmink, A. Verheem, W.J. Van Houdt, E.J. Steller, K.M. Govaert, T.V. Pham, et al., The secretome of colon cancer stem cells contains drug-metabolizing enzymes, J. Proteom. 91 (2013) 84–96.
[45] J. Zhu, H. Wang, Q. Sun, X. Ji, L. Zhu, Z. Cong, et al., Nrf2 is required to maintain the self-renewal of glioma stem cells, BMC Cancer 13 (2013) 380.
[46] H.-J. Kim, A.E. Nel, The role of phase II antioxidant enzymes in protecting memory T cells from spontaneous apoptosis in young and old mice, J. Immunol. 175 (2005) 2948–2959.
[47] A. Kakehashi, N. Ishii, E. Sugihara, M. Gi, H. Saya, H. Wanibuchi, CD44 variant 9 is a potential biomarker of tumor initiating cells predicting survival outcome in hepatitis C virus-positive patients with resected hepatocellular carcinoma, Cancer Sci. 107 (2016) 609–618.
[48] M. Komatsu, H. Kurokawa, S. Waguri, K. Taguchi, A. Kobayashi, Y. Ichimura, et al., The selective autophagy substrate p62 activates the stress responsive transcription factor Nrf2 through inactivation of Keap1, Nat. Cell Biol. 12 (2010) 213–223.
[49] R.Z. Luo, Z.Y. Yuan, M. Li, S.Y. Xi, J. Fu, J. He, Accumulation of p62 is associated with poor prognosis in patients with triple-negative breast cancer, OncoTargets Ther. 6 (2013) 883–888.
[50] Y. Inami, S. Waguri, A. Sakamoto, T. Kouno, K. Nakada, O. Hino, et al., Persistent activation of Nrf2 through p62 in hepatocellular carcinoma cells, J. Cell Biol. 193 (2011) 275–284.
[51] L. Xu, S. Li, W. Zhou, Z. Kang, Q. Zhang, M. Kamran, et al., p62/SQSTM1 enhances breast cancer stem-like properties by stabilizing MYC mRNA, Oncogene 36 (2017) 304–317.
[52] C. Gong, C. Bauvy, G. Tonelli, W. Yue, C. Delomenie, V. Nicolas, et al., Beclin 1 and autophagy are required for the tumorigenicity of breast cancer stem-like/progenitor cells, Oncogene 32 (2013) 2261–2272.
[53] S. Wu, X. Wang, J. Chen, Y. Chen, Autophagy of cancer stem cells is involved with chemoresistance of colon cancer cells, Biochem. Biophys. Res. Commun. 434 (2013) 898–903.
[54] J.L. Guan, A.K. Simon, M. Prescott, J.A. Menendez, F. Liu, F. Wang, et al., Autophagy in stem cells, Autophagy 9 (2013) 830–849.